Eur Radiol (2013) 23:3029–3039
DOI 10.1007/s00330-013-2929-4

HEPATOBILIARY-PANCREAS

Non-hyperfunctioning neuroendocrine tumours of the pancreas: MR imaging appearance and correlation with their biological behaviour

Riccardo Manfredi · Matteo Bonatti · William Mantovani · Rossella Graziani · Diego Segala · Paola Capelli · Giovanni Butturini · Roberto Pozzi Mucelli

Received: 22 December 2012 / Revised: 28 April 2013 / Accepted: 24 May 2013 / Published online: 21 June 2013

Abstract
Objective To describe MR imaging features of non-hyperfunctioning neuroendocrine pancreatic tumours by comparing them to histopathology and to determine the accuracy of MR imaging in predicting biological behaviour.
Materials and Methods After institutional review board approval, we retrospectively reviewed 45 patients with pathologically proven NF-NET of the pancreas and ≥1 preoperative MR/MRCP examinations. Of the NF-NETS, 29/45 (64.4 %) were G1 and 16/45 (35.5 %) were G2. Image analysis included the lesion maximum diameter, vascular encasement, extrapancreatic spread, signal intensity on T1- and T2-weighted, contrast enhancement features, and presence of metastases. Tumour vessel density was calculated on the histological specimen using a grid.
Results The median maximum diameter of NF-NETs was 20 mm (range 5–200 mm). Eighty per cent of the NF-NETs were hypointense on T1-weighted images, 82.2 % were hyperintense on T2-weighted images, and 75.6 % were hypervascular. Overall MRI accuracy showed a mean AUC of 0.86 compared to pathology. Lesions with a maximum diameter of 30 mm irregular margins, absence of a cleavage plane with the main pancreatic duct, vascular encasement, extrapancreatic spread and abdominal metastases were significantly associated with malignant NF-NETs. No correlation was found between the tumour vessel density and contrast-enhanced MR imaging pattern.
Conclusions Hyperintensity on T2-weighted images and iso-/hypervascularity occurred in 27/45 (60.0 %) of NF-NETs. MRI identifies malignant NF-NETs with a sensitivity of 93.3 % and a specificity of 76.9 % (AUC=0.85).
Key Points
- *Non-hyperfunctioning neuroendocrine pancreatic tumours (NF-NET) pose a difficult diagnostic challenge.*
- *On T2-weighted MRI, 82.2 % of neuroendocrine tumours appeared hyperintense.*
- *MR imaging showed 0.94 sensitivity and 0.77 specificity in predicting biological behaviour.*
- *The hyper-/isointensity during dynamic MRI did not correlate with vessel density at pathology.*

Keywords Pancreas · Neoplasms · Neuroendocrine tumours · MR imaging · Biological behaviour · Non-functioning neuroendocrine tumours

R. Manfredi (✉) · M. Bonatti · R. Graziani · R. P. Mucelli
Department of Radiology, University of Verona,
11 P.le L.A. Scuro 10, 37134 Verona, Italy
e-mail: riccardo.manfredi@univr.it

W. Mantovani
Department of Public Health and Community Medicine,
University of Verona, 11 P.le L.A. Scuro 10, 37134 Verona, Italy

D. Segala · P. Capelli
Department of Pathology, University of Verona,
11 P.le L.A. Scuro 10, 37134 Verona, Italy

G. Butturini
Department of Surgery, University of Verona,
11 P.le L.A. Scuro 10, 37134 Verona, Italy

W. Mantovani
Department of Prevention, Public Health Trust APSS,
Trento, Italy

Introduction

Pancreatic neuroendocrine tumours (NETs) originate from ductal pluripotent stem cells and demonstrate endocrine differentiation [1–4], as indicated by the immunohistochemical positivity to chromogranin A and/or to synaptophysin depicted at histopathology [5]. NETs represent 2-10 % of

all pancreatic tumours and can be sporadic or syndromic [6–9]. Clinically pancreatic NETs can be classified into hyperfunctioning and non-hyperfunctioning according to the presence/absence of a distinct clinical syndrome induced by excessive hormone secretion [10–12].

Non-hyperfunctioning neuroendocrine tumours (NF-NET) represent 68-80 % of all pancreatic NETs [13, 14]. Although hormonally silent, NF-NETs may cause symptoms because of the mass effect on adjacent structures [15–17].

The biological behaviour of pancreatic NF-NETs is heterogeneous; therefore they are histologically classified into G1, <2 mitosis per 2 mm^2 [10 high power fields (HPF) 40× magnification] and/or Ki-67 index ≤2 %; G2, 2–20 mitosis per 2 mm^2 and/or Ki-67 index between 3 and 20 %; G3 ≥21 mitosis per 2 mm^2 and Ki-67 index >20 %. G1 and G2 refer to well-differentiated NF-NETs displaying expression of chromogranin A and synaptophysin, whereas G3 indicates a poorly differentiated neuroendocrine carcinoma, with corresponding the 5-year survival rates ranging from 60–100 % for well-differentiated NF-NETs to 29 % for poorly differentiated carcinomas [10, 18–20].

Surgery is the treatment of choice for NF-NET, even in synchronous metastatic disease, if at least 90 % of the tumour mass can be successfully removed [6, 21]. If the tumour is locally unresectable or widely metastatic, locoregional ablative therapies, medical therapy or peptide receptor radionuclide therapy is indicated [6, 21].

From the diagnostic imaging point of view, the medical need is to diagnose and differentiate NF-NETs from other pancreatic tumours, namely adenocarcinoma, to assess their extension and to predict their biological behaviour in order to tailor the most appropriate treatment.

Computed tomography (CT) is the optimal imaging investigation for depicting and assessing the extent of pancreatic NF-NETs [6, 22, 23], whereas magnetic resonance imaging (MRI) is often used as a problem-solving technique, especially for lesion characterisation, because of its higher tissue contrast resolution and its ability to visualise the pancreatic ductal system [24].

The aim of our study was to describe the MR imaging features of NF-NETs by comparing them to histopathological findings and to assess the capability of MR imaging in predicting the biological behaviour of NF-NETs.

Material and methods

Patient population

The institutional review board approved the study and the requirement for informed consent was waived. A search of our institution's medical records and radiological database between January 2004 and January 2011 found 130 patients with diagnoses of NF-NET to be considered for the inclusion in this retrospective study.

Inclusion criteria included surgically resected NF-NET, preoperative MRI/MRCP examination performed at our institution within the 3 months preceding surgery, availability of surgical specimens and histopathological examination of the resected NF-NET.

Exclusion criteria included lack of preoperative MRI/MRCP (44 patients), no surgical procedure being carried out (29 patients), poor image quality (4 patients), von Hippel-Lindau disease (4 patients) and specimens not being available (4 patients).

Thus, our study population encompassed 45 patients with a mean age of 51.2 years (range 25–74 years): 28 females (mean age 51.2 years; range 25–74 years) and 17 males (mean age 50.7 years; range 25–73 years).

At diagnosis, 21/45 (46.7 %) patients were asymptomatic, whereas 24/45 (53.3 %) were symptomatic. Symptoms were abdominal pain in 12/24 (50.0 %), weight loss in 9/24 (37.5 %), diabetes in 7/24 (29.2 %), jaundice in 3/24 (12.5 %) and acute pancreatitis in 3/24 (12.5 %) patients, with 9 patients presenting with more than one symptom.

All patients underwent preoperative MR/MRCP imaging and surgical procedures. The median time interval between MR/MRCP and surgery was 1.2 months (range 0.1–2.8 months).

Magnetic resonance imaging

MR imaging was performed at 1.5 T (Magnetom Symphony, Siemens, Erlangen, Germany) using a four-channel phased array coil.

The patients were asked to fast 4–6 h before the examination. Furthermore, to eliminate overlapping fluid-containing organs on T2-weighted images, 50–150 ml of superparamagnetic iron oxide particles (ferumoxsil, Lumirem, Guerbet, Aulnay-sous-Bois, France) were administered 10–20 min before MRI.

The MR imaging protocol and pulse sequence parameters are reported in Table 1.

The dynamic study, during gadolinium-chelate injection, was obtained by means of a 3D volumetric gradient echo pulse sequence (VIBE, volumetric interpolated breath-hold examination) using parallel imaging (GRAPPA acceleration factor 2) when available. A quadriphasic dynamic study was performed during 0.1 mmol/kg body weight gadolinium-chelate injection (Multihance, Bracco, Milan, Italy, or Dotarem, Guerbet, Aulnay-sous-Bois, France) by means of a power injector (Spectris, Medrad, Pittsburgh, PA, USA) at 2–2.5 ml/s by acquiring the pre-contrast-phase, late arterial/pancreatic phase (35–45 s), portal venous phase (75–80 s) and equilibrium-delayed phase (>180 s).

Table 1 Magnetic resonance (MR) imaging protocol: pulse sequences and parameters

Pulse sequence	Plane	TR (ms)	TE (ms)	Slice thickness (mm)
Chemical shift T1-weighted gradient echo	Axial	107–160	2.4–4.8	7–8
Fat-saturated T2-weighted (RARE)	Axial	4,000–4,950	91–102	7–8
T2-weighted half Fourier RARE (HASTE)	Coronal and axial	∞	60–102	4–6
T2-weighted half Fourier RARE (HASTE)	Coronal	∞	102–400	40–60
2D half Fourier RARE (HASTE) MRCP	Multiple	∞	1,100	40–80
Fat-saturated 3D volumetric gradient echo (VIBE)	Axial	4.66	1.87	2.6–3

TR, Repetition time; TE, echo time; RARE, rapid acquisition with relaxation enhancement; HASTE, half Fourier single-shot turbo spin-echo; MRCP, magnetic resonance cholangiopancreatography; VIBE, volumetric interpolated breath-hold examination; 2D, two dimensional; 3D, three dimensional

Image analysis

Qualitative image analysis. MR/MRCP images were independently analysed on a workstation by two radiologists (RM and RPM; 18 and 30 years of experience in gastrointestinal radiology, respectively) who were aware of the diagnosis of NET but unaware of the surgical/pathological evaluation of the lesion. Discrepancies were solved by consensus. Image analysis included the site of the pancreatic NF-NET (head, body/tail or diffuse), lesion margins (sharp or irregular), signal intensity on T1-WI and T2-WI related to the adjacent pancreatic parenchyma (hypo-, iso- or hyperintense), contrast enhancement of the neoplasm during the arterial/pancreatic and portal venous phase of the dynamic study compared to the adjacent parenchyma (hypo-, iso- or hyperintense), signal intensity of the

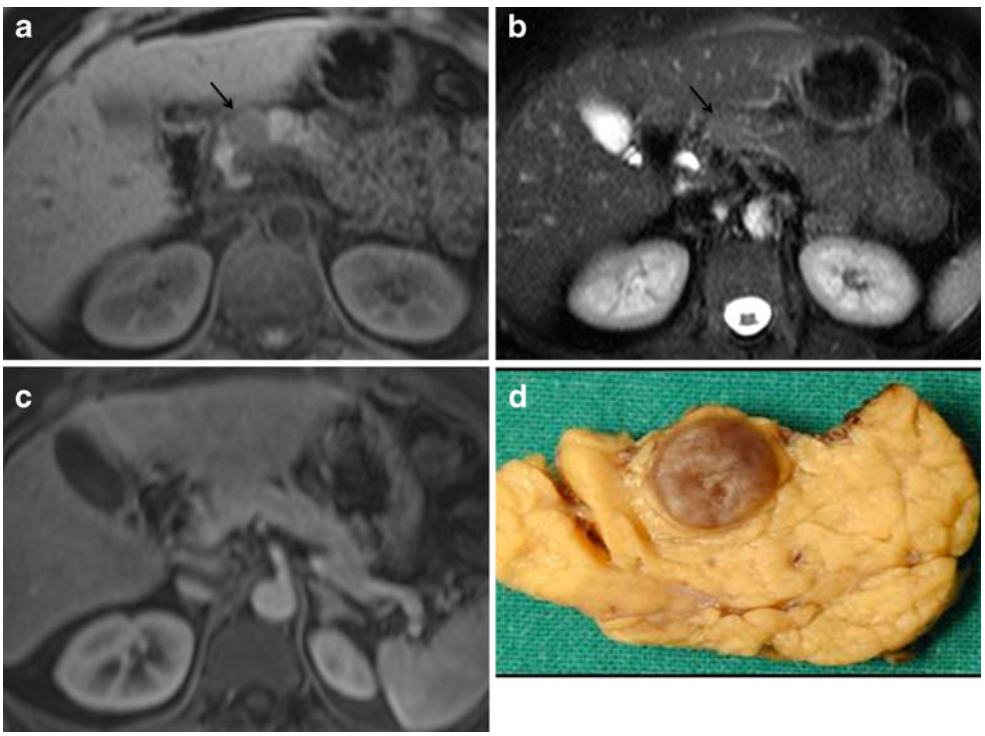

Fig. 1 **a-c** Small non-functioning neuroendocrine tumour (NF-NET) of the pancreas classified as adenoma at histology. **a** Axial fat-saturated volumetric interpolated breath-hold examination (VIBE) gradient echo image (TR/TE 4.66/1.87 ms) shows an homogeneously hypointense non-functioning neuroendocrine tumour (NF-NET), with sharp margins in the head-isthmus of the pancreas, left to the superior mesenteric vein. **b** On axial fat-saturated T2-weighted rapid acquisition with relaxation enhancement (RARE) image (TR/TE 4,500/100 ms), the NF-NET appears slightly hyperintense compared to adjacent pancreatic parenchyma. The NF-NET presented a maximum diameter of 29 mm and no signs of either extrapancreatic spread or vascular encasement, suggesting benign behaviour. **c** On axial fat-saturated volumetric interpolated breath-hold examination (VIBE) gradient echo image (TR/TE 4.66/1.87 ms), acquired during the arterial/pancreatic phase of the dynamic study, the NF-NET appears isointense compared to adjacent pancreatic parenchyma. **d** The macroscopic pathological specimen, following middle pancreatectomy, shows a well-delimitated, brown, round non-hyperfunctioning neuroendocrine tumour (NF-NET) of the pancreas, classified as adenoma, at histology

neoplasm during the delayed phase compared to the portal venous phase (washout/retention), encasement of the mesenteric vessels and coeliac trunk (present/absent), extrapancreatic spread [involvement of the peri-pancreatic fat (present/absent)], the relationship with the main pancreatic duct (MPD) (cleavage plane or compression/infiltration) and presence of liver metastases.

Quantitative image analysis was performed by a third radiologist not involved in the qualitative analysis (MB, 4 years of experience) on a workstation using an

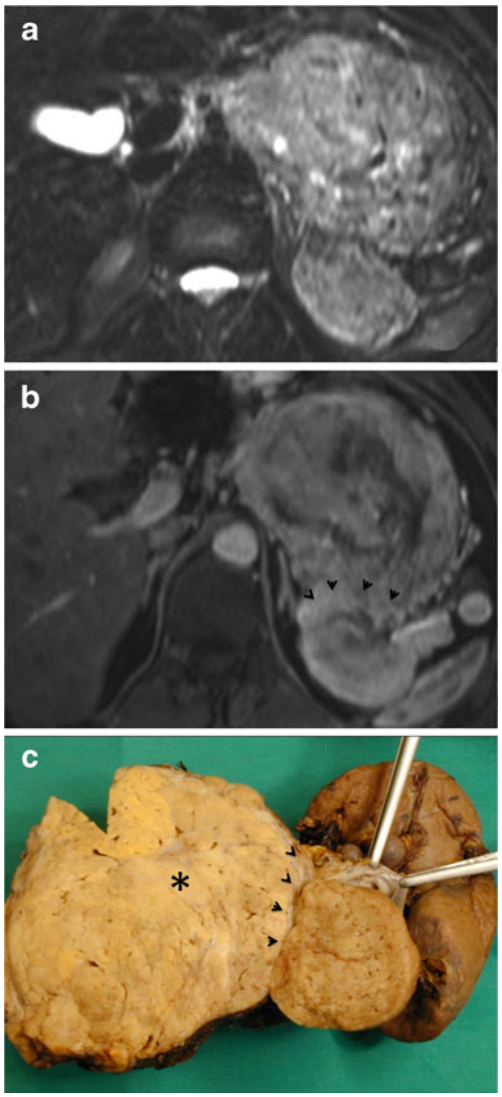

Fig. 2 **a-c** Malignant non-functioning neuroendocrine tumour (NF-NET) of the body-tail of the pancreas, with signs of extrapancreatic spread classified as high-grade carcinoma at histology. **a** Axial fat-saturated T2-weighted rapid acquisition with relaxation enhancement (RARE) image (TR/TE 4,500/100 ms) shows an NF-NET in the body-tail of the pancreas, which appears heterogeneously hyperintense on T2-WI; in addition multiple strongly hyperintense central areas can be observed, suggesting liquefaction. **b** On axial fat-saturated T1-weighted volumetric interpolated breath-hold examination (VIBE) gradient echo image (TR/TE 4.66/1.87 ms) acquired during the portal venous phase of the dynamic study shows heterogeneous contrast enhancement of the NF-NET, with a hypointense central area, suggesting necrosis. The NF-NET shows extrapancreatic spread with infiltration of the left kidney (*arrowheads*). **c** The surgical specimen (en bloc spleno-pancreatectomy and resection of the left kidney) shows a large lesion of the body-tail of the pancreas (*) with irregular margins infiltrating the left kidney (*arrowheads*); at histology the neoplasm was classified as high-grade malignant NF-NET of the pancreas

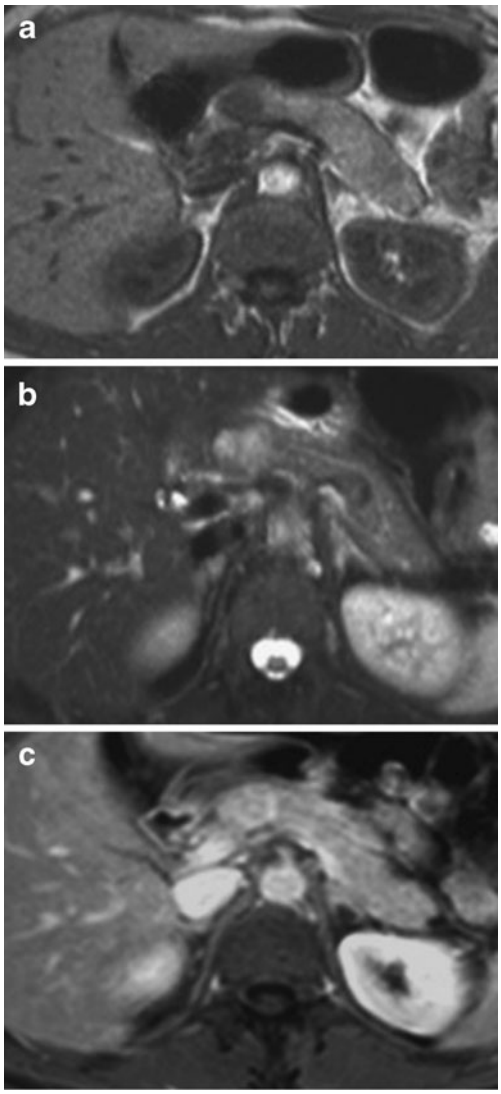

Fig. 3 **a-c**. Malignant non-functioning neuroendocrine tumour (NF-NET) of the head of the pancreas without diagnostic imaging findings of malignancy. **a** This 18-mm-large lesion of the head of the pancreas appeared hypointense on T1-weighted gradient echo (GRE) image (TR/TE/ 160/2.8 ms) and hyperintense on fat-saturated T2-weighted rapid acquisition with relaxation enhancement (RARE) image (TR/TE 4,500/100 ms). **b** The lesion shows sharp margins and homogeneous structure. **c** On axial fat-saturated T1-weighted volumetric interpolated breath-hold examination (VIBE) gradient echo image (TR/TE 4.66/1.87 ms), acquired during the arterial/pancreatic phase of the dynamic study, the NF-NET appears heterogeneously hyperintense. The MR imaging pattern suggests a benign/borderline NF-NET; at histo-pathology, however, the neoplasm was classified as low-grade malignant NF-NET because of its high mitotic index

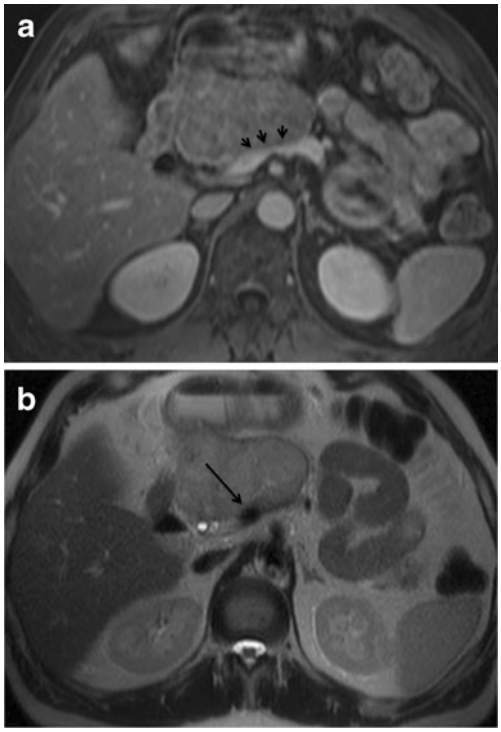

Fig. 4 **a-b** Malignant non-functioning diffuse neuroendocrine tumour (NF-NET) of the pancreas with peri-pancreatic vessel infiltration. **a** Axial fat-saturated T1-weighted volumetric interpolated breath-hold examination (VIBE) gradient echo image (TR/TE 4.66/1.87 ms) acquired during the portal venous phase of the dynamic study shows an NF-NET involving both the head and body of the pancreas, with extrapancreatic spread and infiltration of the spleno-mesenteric confluence (*arrowheads*) confirmed at histopathology. **b** The axial T2-weighted half Fourier image (HASTE) shows a wide contact between the NF-NET and the spleno-mesenteric confluence with endoluminal flow void (*arrow*), suggesting vessel wall infiltration without occlusion, indicative of malignant NF-NET, which was confirmed at histopathology

electronic calibre and included the maximum diameter of the lesion.

Pathology specimen analysis

The pathologist (DS, 6 years of experience) was asked to review the specimens of each patient using the same criteria used for the radiological evaluation and to classify the lesion according to the grading and TNM classification [20]. Furthermore, quantification of microvessel density (MVD) was performed by calculating the percentage of the vessel area, which reflects MVD. All sections taken from the greatest tumour diameter were immunostained with the anti-CD34 antibody (QBEND10; Novocastra, Burlingame CA, USA) by using an automated bond polymer refine detection system (Leica Byosystems, Newcastle Ltd., UK). The areas of highest vascularisation were found by scanning the sections at 40× and 100× magnification. For each tumour, three computerised images with a surface of 1 mm^2 were obtained at a 100× magnification, and a reticule that contained 100 points was applied to each computerised image. Vessels coinciding with the points were counted, and the result was expressed as a percentage of area.

All radiological findings were compared to pathological data by a radiologist (MB) and a pathologist (PC, 25 years of experience).

Statistical analysis

Interobserver variability of the qualitative image analysis was assessed by means of κ statistics. The strength of agreement was assessed as poor if $\kappa<0.20$, fair if $\kappa=0.21–0.40$, moderate if $\kappa=0.41–0.60$, good if $\kappa=0.61–0.80$ and excellent if $\kappa=0.81–1.00$.

The distributions of continuous variables are reported as mean (and/or median) values and range (minimum and maximum values). Categorical variables are presented as numbers and percentages. The main outcome considered

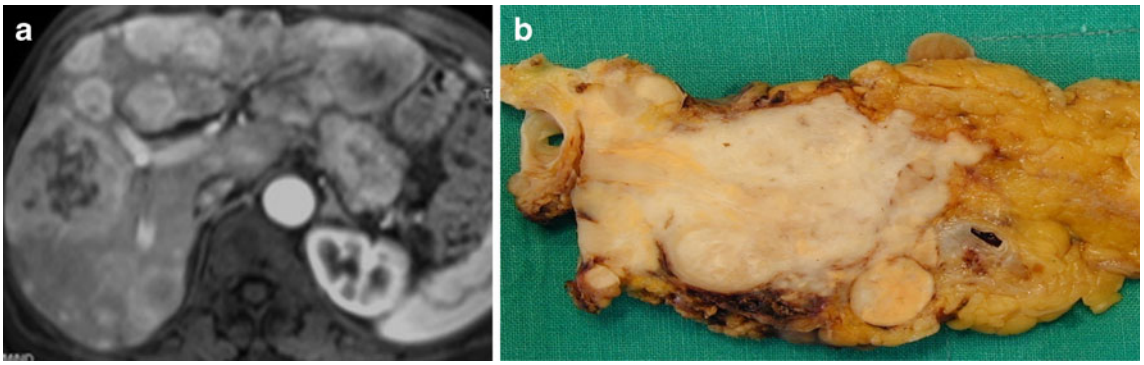

Fig. 5 **a-b** Malignant non-functioning neuroendocrine tumour (NF-NET) of the body/tail of the pancreas with liver metastases. **a** On axial fat-saturated T1-weighted volumetric interpolated breath-hold examination (VIBE) gradient echo image (TR/TE 4.66/1.87 ms) acquired during the arterial/pancreatic phase of the dynamic study, the NF-NET appears heterogeneously hyperintense compared to the adjacent parenchyma (*arrow*) and shows signs of extrapancreatic spread. Moreover, multiple hyperintense liver metastases are present. **b** The surgical specimen (distal pancreatectomy) shows a lesion of the tail of the pancreas with irregular margins suggesting an infiltrating growth pattern. At histology the neoplasm was classified as high-grade malignant NF-NET of the pancreas

was the histopathological diagnosis of poorly differentiated carcinoma. For data analysis, patients presenting liver metastases at MRI were not included, their NF-NETs being certainly malignant, without any need for further evaluation.

The comparison between subgroups (G1 vs. G2 vs. G3, as well as TNM stage I/II vs. III/IV) was performed with Student's *t* test and the Mann–Whitney *U* test for continuous variables. Qualitative data were compared with the $\chi 2$ or Fisher's exact tests when necessary.

Diagnostic accuracy was assessed as the area under the receiver-operating characteristic (ROC) curve. Diagnosis obtained by pathologic examination was the external gold standard. Sensitivity, specificity and area under curve (AUC) (and their 95 % confidence intervals) for each significant parameter in the prediction of malignancy were also calculated [25, 26]. AUC values <0.60 indicated failed accuracy, 0.61–0.70 poor accuracy, 0.71–0.80 fair accuracy, 0.81–0.90 good accuracy and 0.91–1.00 excellent accuracy.

All tests were two sided. *P* values≤0.05 were considered statistically significant.

Results

MR imaging

Qualitative image analysis

NF-NETs were located in the head of the pancreas in 22/45 (48.9 %) of the patients and in the body/tail in 14/45 (31.1 %), whereas 9/45 (20.0 %) patients showed a diffuse involvement of the gland (k=0.98). Lesion margins were sharp in 30/45 (66.7 %) of the cases and irregular in 15/45 (33.3 %) (k=0.84) (Figs. 1, 2, and 3).

On T1-weighted images, NF-NETs were hypointense compared to the adjacent parenchyma in 36/45 (80.0 %) patients (Figs. 1, 2, and 3) and isointense in the remaining 9/45 (20.0 %) (k=0.92). On T2-weighted images, they appeared hyperintense in 37/45 (82.2 %) of patients (Figs. 1, 2, 3, and 4), isointense in 5/45 (11.1 %) and hypointense in 3/45 (6.7 %) (k=0.87).

During the arterial/pancreatic phase of the dynamic study, NF-NETs appeared hyperintense compared to the adjacent parenchyma in 27/45 (60.0 %) patients (Fig. 3), hypointense in 11/45 (24.4 %) and isointense in 7/45 (15.6 %) (k=0.87) (Fig. 1). During the portal venous phase NF-NETs appeared hyperintense in 26/45 (56.8 %) patients (Fig. 2), hypointense in 11/45 (24.4 %) and isointense in 8/45 (17.8 %) (k=0.89). During the delayed phase, the neoplasms showed retention in 26/45 (57.8 %) compared to the previous portal venous phase and washout in 18/45 (40.0 %) of the cases; in 1/45 (2.2 %) patients the delayed phase was not available (k=0.85).

A sub-analysis showed that 27/45 (60.0 %) of NF-NETs appeared both hyperintense on T2-weighted images and iso-/hyperintense during the arterial/pancreatic phase of the dynamic study, representing the most frequent pattern at MR imaging in our series (Figs. 1, 2, and 3). One of 45 (2.2 %) NF-NETs appeared both hypointense on T2-weighted images and hypointense during the arterial/pancreatic phase of the dynamic study, representing a difficult differential diagnosis with pancreatic adenocarcinoma.

Vascular encasement was present in 12/45 (26.7 %) of the cases and absent in 33/45 (73.3 %) (k=0.82) (Fig. 4). Extrapancreatic spread was present in 11/45 (24.4 %) of the NF-NETs and absent in 34/45 (75.6 %) (k=0.84) (Figs. 2, 4 and 5).

The main pancreatic duct was compressed/infiltrated in 29/45 (64.4 %) cases and not involved in 16/45 (35.6 %) (k=0.74). Dilatation of the upstream main pancreatic duct was present in 15/45 (33.3 %) of the cases and absent in 25/45 (55.6 %). In 5/45 (11.1 %) cases the upstream MPD was impossible to evaluate because of the location of the neoplasm in the tail of the gland. The suprapancreatic

Table 2 Sensitivity and specificity of magnetic resonance (MR) with MR cholangiopancreatography (MRCP) (MR/MRCP) in the assessment of qualitative imaging parameters of NF-NETs compared to histopathology. Absolute values and 95 % confidence intervals (CI) are reported; the area under the curve (AUC) represents the summary parameter

	Sensitivity (95 % CI)	Specificity (95 % CI)	AUC (95 % CI)
Lesion margins	0.81 (0.54–0.96)	0.93 (0.77–0.99)	0.87 (0.74–0.95)
Vascular encasement	0.92 (0.62–1.0)	0.97 (0.84–1.0)	0.94 (0.83–0.99)
Extrapancreatic spread	0.58 (0.28–0.85)	0.88 (0.72–0.97)	0.73 (0.58–0.85)
MPD involvement	0.87 (0.69–0.96)	0.80 (0.52–0.96)	0.83 (0.72–0.95)
Upstream MPD dilatation	0.93 (0.66–1.0)	0.94 (0.79–0.99)	0.93 (0.82–0.99)
CBD dilatation	0.67 (0.22–0.96)	1.0 (0.91–1.0)	0.83 (0.69–0.93)

MPD, main pancreatic duct; CBD, common main duct; AUC, area under the curve

common bile duct showed a normal calibre in 41/45 (91.1 %) of the cases, whereas it appeared dilated in 4/45 (8.9 %). Liver metastases were present in 4/45 (8.9 %) patients and absent in 41/45 (91.1 %) (k=1.0) (Fig. 5).

Table 3 Univariate analysis involving the 41/45 lesions without evidence of abdominal metastases at MRI. Association between the different MRI patterns of NF-NETs and their biological behaviour, expressed by tumour grading, is shown. The strength of the association is quantified by means of the P value (significant association if $P < 0.05$)

	Grading				P
	G1 (n=29)		G2 (n=16)		
	n	% Cases/ row	n	% Cases/ row	
Diameter of the neoplasm					
<30 mm	22	88.0 %	3	12.0 %	<0.0001
≥30 mm	7	43.8 %	9	56.3 %	
Location					
Head	19	90.5 %	2	9.5 %	0.123
Body/tail	4	36.4 %	7	63.6 %	
Diffuse	6	66.7 %	3	33.3 %	
Margins					
Sharp	21	75.0 %	7	25.0 %	0.084
Irregular	8	61.5 %	5	38.5 %	
MPD relation					
Normal	14	93.3 %	1	6.7 %	0.002
Infiltration	15	57.7 %	11	42.3 %	
Upstream MPD					
Normal	20	74.1 %	7	25.9 %	0.105
Dilated	9	64.3 %	5	35.7 %	
Upstream CBD					
Normal	27	73.0 %	10	27.0 %	0.637
Dilated	2	50.0 %	2	50.0 %	
Vascular encasement					
Absent	27	84.4 %	5	15.6 %	0.001
Present	2	22.2 %	7	77.8 %	
Local spread					
Absent	28	84.8 %	5	15.2 %	0.006
Peripancreatic fat	1	20.0 %	4	80.0 %	
Adjacent organs	0	0.0 %	3	100.0 %	
Signal intensity on T1-WI					
Hypointense	22	64.7 %	12	35.3 %	0.215
Isointense	7	100.0 %	0	0.0 %	
Hyperintense	0	0.0 %	0	0.0 %	
Signal intensity on T2-WI					
Hypointense	1	50.0 %	1	50.0 %	0.143
Isointense	3	60.0 %	2	40.0 %	
Hyperintense	25	73.5 %	9	26.5 %	
Signal intensity on arterial/pancreatic phase					
Hypointense	7	70.0 %	3	30.0 %	0.568
Isointense	5	71.4 %	2	28.6 %	
Hyperintense	17	70.8 %	7	29.2 %	
Signal intensity on portal venous phase					
Hypointense	5	45.5 %	6	54.5 %	0.398
Isointense	6	75.0 %	2	25.0 %	
Hyperintense	18	81.8 %	4	18.2 %	
Delayed phase					
Washout	9	52.9 %	8	47.1 %	0.255
Retention	19	82.6 %	4	17.4 %	
Not evaluable	1	100.0 %	0	0.0 %	

MPD, Main pancreatic duct; CBD, common bile duct; SI, signal intensity; T1-WI, T1-weighted images; T2-WI, T2-weighted images

Table 4 Univariate analysis involving the 41/45 lesions without evidence of abdominal metastases at MRI. Association between the different MRI patterns of NF-NETs and TNM stage is shown. The strength of the association is quantified by means of the *P* value (significant association if $P<0.05$)

	TNM stage cluster				*P*
	I-IIa-IIb ($n=32$)		IIIa-IIIb-IV ($n=13$)		
	n	% Cases/ row	*n*	% Cases/ row	
Diameter of the neoplasm					
<30 mm	21	84.0 %	4	16.0 %	
≥30 mm	4	25.0 %	12	75.0 %	
Location					
Head	16	76.2 %	5	23.8 %	0.123
Body/tail	5	45.5 %	6	54.5 %	
Diffuse	4	44.4 %	5	55.6 %	
Margins					
Sharp	20	71.4 %	8	28.6 %	0.084
Irregular	5	38.5 %	8	61.5 %	
MPD relation					
Normal	14	93.3 %	1	6.7 %	0.002
Infiltration	11	42.3 %	15	57.7 %	
Upstream MPD					
Normal	19	70.4 %	8	29.6 %	0.105
Dilated	6	42.9 %	8	57.1 %	
Upstream CBD					
Normal	23	62.2 %	14	37.8 %	0.637
Dilated	2	50.0 %	2	50.0 %	
Vascular encasement					
Absent	24	75.0 %	8	25.0 %	0.001
Present	1	11.1 %	8	88.9 %	
Local spread					
Absent	24	72.7 %	9	27.3 %	0.006
Peripancreatic fat	1	20.0 %	4	80.0 %	
Adjacent organs	0	0.0 %	3	100.0 %	
Signal intensity on T1-WI					
Hypointense	19	55.9 %	15	44.1 %	0.215
Isointense	6	85.7 %	1	14.3 %	
Hyperintense	0	0.0 %	0	0.0 %	
Signal intensity on T2-WI					
Hypointense	0	0.0 %	2	100.0 %	0.143
Isointense	4	80.0 %	1	20.0 %	
Hyperintense	21	61.8 %	13	38.2 %	
Signal intensity on arterial/pancreatic phase					
Hypointense	7	70.0 %	3	30.0 %	0.568
Isointense	5	71.4 %	2	28.6 %	
Hyperintense	13	54.2 %	11	45.8 %	
Signal intensity on portal venous phase					
Hypointense	5	45.5 %	6	54.5 %	0.398
Isointense	6	75.0 %	2	25.0 %	
Hyperintense	14	63.6 %	8	36.4 %	
Delayed phase					
Washout	9	52.9 %	8	47.1 %	0.255
Retention	16	69.6 %	7	30.4 %	
Not evaluable	0	0.0 %	1	100.0 %	

MPD, Main pancreatic duct; CBD, common bile duct; SI, signal intensity; T1-WI, T1-weighted images; T2-WI, T2-weighted images

Quantitative image analysis

NF-NETs presented a mean maximum diameter of 39 mm (range 5 – 200 mm), with a median value of 20 mm.

MR imaging-pathological correlation

At pathology, 25/45 (55.6 %) neoplasms were located in the head of the pancreas, 12/45 (26.7 %) in the body/tail, and

8/45 (17.8 %) showed diffuse involvement of the gland. Lesion margins were sharp in 29/45 (64.4 %) of the cases (Fig. 1) and irregular in 16/45 (35.6 %) (Figs. 2 and 5). Vascular encasement was present in 12/45 (26.7 %) of the cases and absent in 33/45 (73.3 %). Extrapancreatic spread was present in 13/45 (28.9 %) and absent in 32/45 (71.1 %) (Fig. 2). The main pancreatic duct was compressed/infiltrated in 29/45 (64.4 %) of the cases and not involved in 16/45 (35.6 %). Dilation of the upstream main pancreatic duct was present in 15/45 (33.3 %) of the cases, absent in 25/45 (55.6 %) and not evaluable in 5/45 (11.1 %). The suprapancreatic common bile duct presented a normal calibre in 41/45 (91.1 %) cases and was dilated in 4/45 (8.9 %).

At surgery, 32 patients had localised NF-NETs: 19 stage I, 7 stage IIa and 6 stage IIb. Thirteen patients had locally advanced disease: 7 stage IIIb and 6 stage IV [20]. The pathologist classified the neoplasms as G1 in 29/45 (64.4 %) of the cases and G2 in 16/45 (35.5 %) of the cases.

NF-NET showed a mean intralesional vessel density of 9.8 (range 5.0–42.7). Benign/border line NF-NET showed a mean vessel density of 12.7 (range 5.0-42.7). Malignant NF-NET showed a mean vessel density of 9.4 (range 5.0–15.0). No significant correlation was found between the vessel density and signal intensity of the NF-NETs during either the arterial/pancreatic or portal venous phase of the dynamic study.

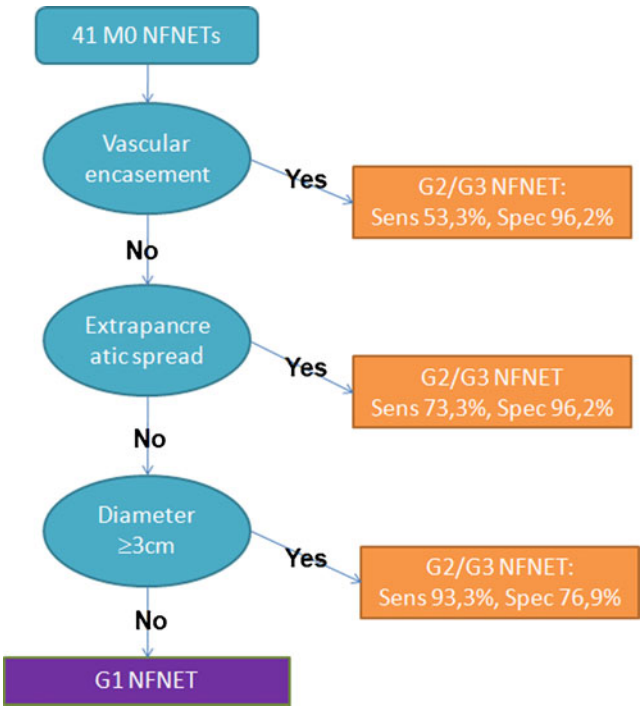

Fig. 6 Suggested "three-step" diagnostic flow chart for risk stratification of the biological behaviour (G1 vs. G2/G3) of non-functioning neuroendocrine tumours (NF-NETs) as deducted from the observation of 41 patients. Four patients with metastatic NF-NETs (M+) were excluded from the analysis

At surgery, liver metastases were detected in 4/45 (8.9 %) patients.

The agreement between qualitative image analysis as detected on MR/MRCP images and histopathology is reported in Table 2. Namely, the sensitivity and specificity of MR imaging and the values of the area under the curve (AUC) for each parameter are reported.

Prediction of malignancy For this sub-analysis 4/45 (8.9 %) patients presenting liver metastases were not included.

The results of the univariate analysis attempting to identify MR/MRCP imaging parameters predictive of the biological behaviour of NF-NETs (i.e. G1 vs. G2; TNM stage I/II vs. stage III/IV) are reported in Tables 3 and 4. In our series, a significant predictive value of aggressive behaviour of the neoplasm was identified for the maximum diameter of the neoplasm ($P<0.001$), presence of vascular encasement ($P=0.001$), vascular encasement ($P=0.001$), presence of extrapancreatic spread ($P=0.006$) and absence of a cleavage plane with the MPD ($P=0.002$).

Discussion

One of the medical needs in diagnostic imaging of non-hyperfunctioning neuroendocrine tumours (NF-NETs) is the differential diagnosis between NF-NETs and pancreatic adenocarcinoma when a solid mass is detected at diagnostic imaging, since overall the 5-year survival for NF-NETs is 30–63 % [6], whereas for pancreatic adenocarcinoma it is 5 % [27]. According to our series, the MR imaging sign suggestive of NF-NETs is hyperintensity on T2-weighted images, which was detected in 82.2 % of the patients (37/45), in contrast to adenocarcinoma, which appears hypointense on all pulse sequences because of its scirrhous feature.

Another MR imaging feature helpful in the characterisation of NF-NETs is the hyperintensity or isointensity during the arterial/pancreatic phase of the dynamic study, encompassing 75.5 % (34/45) of lesions in our series, in contrast to adenocarcinoma, which appears hypointense during the arterial/pancreatic phase in 89 % of the cases [28]. Furthermore, when we combine the two above-mentioned parameters (i.e. hyperintensity on T2-WI and hyper-/isointensity during the arterial/pancreatic phase), 27/45 (60.0 %) of the patients in our series showed this pattern, whereas only 1/45 (2.2 %) NF-NETs appeared both hypointense on T2-weighted images and hypointense during the arterial/pancreatic phase of the dynamic study, becoming impossible to differentiate from pancreatic adenocarcinoma.

In our series, the MR imaging pattern, as depicted during the arterial/pancreatic phase of the dynamic study, did not

correlate with the mean vessel density, as observed on the pathological specimen, suggesting that the diagnostic imaging appearance during the dynamic study is most likely the result of different factors, such as blood flow, blood volume and permeability, in addition to mean vessel density [29].

In the evaluation of morphological aspects of NF-NETs, MRI showed an AUC curve of 0.86 compared to histopathology and therefore can be considered an accurate method for the prediction of pathological findings in NF-NETs. The single evaluated parameters presented AUC values ranging from 0.73 (presence of extrapancreatic spread) to 0.94 (presence of vascular encasement).

The treatment of choice for NF-NETs is surgical resection, which should always be performed if technically feasible, even in case of metastatic disease, because of the quite favourable prognosis of these neoplasms. The surgical strategy, however, can differ according to tumour location (considering its anatomical position and its relation with MPD) and tumour size, but also according to its potential malignancy. The surgical options range from a simple tumour enucleation, which, however, is only considered to be curative for adenomas and borderline lesions, to partial or total pancreatectomy, which is necessary in order to reach a curative intent in case of carcinoma [6]. Therefore, it is important to give the surgeons information about not only the location and the size of NF-NET, but also the risk of malignant behaviour. In this setting, besides the well-established criteria of malignancy such as the presence of metastases, extrapancreatic spread, vascular encasement and irregular margins, the parameter associated with malignancy is tumour size, in agreement with other published series [30]. In our series, the mean size of benign/borderline NF-NETs (20 mm) was statistically lower (<0.001) compared to malignant NF-NETs (70 mm).

All these parameters, however, if independently considered showed a low sensitivity in the detection of malignancy, with values ranging from 21.0 % (presence of abdominal metastases) to 57.9 % (presence of vascular encasement), the latter most likely related to the fact that neuroendocrine tumours are responsible for neoplastic venous thrombosis rather than vascular encasement [31]. In order to try to improve the sensitivity in the identification of malignant NF-NETs, we combined the malignancy-correlated parameters together, suggesting a "three-step" flow chart (Fig. 6). By applying this diagnostic algorithm, a sensitivity of 0.93 and specificity of 0.77 in the identification of malignant lesions and an AUC of 0.85 in the identification of malignant NF-NETs can be achieved. The relation between the neoplasm and the main pancreatic duct (compressed/infiltrated vs. not involved) was not included in this algorithm because, although strongly concordant with pathological findings (AUC=0.83) and significantly correlated with malignancy (P=0.003), it was the only parameter that did not show high concordance in the interobserver agreement (k=0.74).

Our study has several limitations that the authors are well aware of, mainly related to the retrospective design of the study: the most noticeable is a selection bias in the patient population, since in the study we only included patients with proven NF-NET who underwent surgery.

In conclusion, non-hyperfunctioning neuroendocrine pancreatic tumours showed magnetic resonance imaging features such as hyperintensity on T2-weighted images and hyper-/isointensity during the arterial/pancreatic phase of enhancement that are helpful in making the differential diagnosis of solid pancreatic masses. MR imaging showed a sensitivity of 93.3 % and specificity of 76.9 % (AUC=0.85) in assessing features useful for treatment planning, such as vascular encasement and extrapancreatic spread, when compared to histopathology.

References

1. Gumbs AA, Moore PS, Falconi M et al (2002) Review of the clinical, histological, and molecular aspects of pancreatic endocrine neoplasms. J Surg Oncol 81:45–53, discussion 54
2. Zerbi A, Falconi M, Rindi G et al (2010) Clinicopathological features of pancreatic endocrine tumors: a prospective multicenter study in Italy of 297 sporadic cases. Am J Gastroenterol 105:1421–1429
3. Ramage JK, Ahmed A, Ardill J et al (2012) Guidelines for the management of gastroenteropancreatic neuroendocrine (including carcinoid) tumours (NETs). Gut 61:6–32
4. Capelli P, Martignoni G, Pedica F et al (2009) Endocrine neoplasms of the pancreas: pathologic and genetic features. Arch Pathol Lab Med 133:350–364
5. Capella C, Heitz PU, Hofler H, Solcia E, Kloppel G (1995) Revised classification of neuroendocrine tumours of the lung, pancreas and gut. Virchows Arch: Int J Pathol 425:547–560
6. Falconi M, Plockinger U, Kwekkeboom DJ et al (2006) Well-differentiated pancreatic nonfunctioning tumors/carcinoma. Neuroendocrinology 84:196–211
7. Barakat MT, Meeran K, Bloom SR (2004) Neuroendocrine tumours. Endocr Relat Cancer 11:1–18
8. Marcos HB, Libutti SK, Alexander HR et al (2002) Neuroendocrine tumors of the pancreas in von Hippel-Lindau disease: spectrum of appearances at CT and MR imaging with histopathologic comparison. Radiology 225:751–758
9. Bilimoria KY, Tomlinson JS, Merkow RP et al (2007) Clinicopathologic features and treatment trends of pancreatic neuroendocrine tumors: analysis of 9,821 patients. J Gastrointest Surg: Off J Soc Surg Aliment Tract 11:1460–1467, discussion 1467–1469
10. Plockinger U, Rindi G, Arnold R et al (2004) Guidelines for the diagnosis and treatment of neuroendocrine gastrointestinal tumours. A consensus statement on behalf of the European Neuroendocrine Tumour Society (ENETS). Neuroendocrinology 80:394–424
11. Plockinger U, Wiedenmann B (2004) Diagnosis of non-functioning neuro-endocrine gastro-enteropancreatic tumours. Neuroendocrinology 80:35–38
12. Chang S, Choi D, Lee SJ et al (2007) Neuroendocrine neoplasms of the gastrointestinal tract: classification, pathologic basis, and imaging features. Radiographics: a Review Publication of the Radiological Society of North America, Inc 27:1667–1679

13. Pape UF, Bohmig M, Berndt U, Tiling N, Wiedenmann B, Plockinger U (2004) Survival and clinical outcome of patients with neuroendocrine tumors of the gastroenteropancreatic tract in a German referral center. Ann N Y Acad Sci 1014:222–233
14. Corleto VD, Panzuto F, Falconi M et al (2001) Digestive neuroendocrine tumours: diagnosis and treatment in Italy. A survey by the Oncology Study Section of the Italian Society of Gastroenterology (SIGE). Dig Liver Dis: Off J Ital Soc Gastroenterol Ital Assoc Study Liver 33:217–221
15. Madura JA, Cummings OW, Wiebke EA, Broadie TA, Goulet RL Jr, Howard TJ (1997) Nonfunctioning islet cell tumors of the pancreas: a difficult diagnosis but one worth the effort. Am Surg 63:573–577, discussion 577–578
16. Matthews BD, Heniford BT, Reardon PR, Brunicardi FC, Greene FL (2000) Surgical experience with nonfunctioning neuroendocrine tumors of the pancreas. Am Surg 66:1116–1122, discussion 1122–1113
17. White TJ, Edney JA, Thompson JS, Karrer FW, Moor BJ (1994) Is there a prognostic difference between functional and nonfunctional islet cell tumors? Am J Surg 168:627–629, discussion 629–630
18. Solcia E, Kloppel G, Sobin LH (2000) Histological typing of endocrine tumors. Springer, New York
19. Klimstra DS, Modlin IR, Adsay NV et al (2010) Pathology reporting of neuroendocrine tumors: application of the Delphic consensus process to the development of a minimum pathology data set. Am J Surg Pathol 34:300–313
20. Rindi G, Kloppel G, Alhman H et al (2006) TNM staging of foregut (neuro)endocrine tumors: a consensus proposal including a grading system. Virchows Arch: Int J Pathol 449:395–401
21. Franko J, Feng W, Yip L, Genovese E, Moser AJ Non-functional neuroendocrine carcinoma of the pancreas: incidence, tumor biology, and outcomes in 2,158 patients. J Gastrointest Surg 14(3):541–548
22. Graziani R, Brandalise A, Bellotti M et al (2010) Imaging of neuroendocrine gastroenteropancreatic tumours. La Radiologia Medica 115:1047–1064
23. Rockall AG, Reznek RH (2007) Imaging of neuroendocrine tumours (CT/MR/US). Best Pract Res Clin Endocrinol Metab 21:43–68
24. Owen NJ, Sohaib SA, Peppercorn PD et al (2001) MRI of pancreatic neuroendocrine tumours. Br J Radiol 74:968–973
25. Knottnerus JA, van Weel C, Muris JW (2002) Evaluation of diagnostic procedures. BMJ 324:477–480
26. Zweig MH, Campbell G (1993) Receiver-operating characteristic (ROC) plots: a fundamental evaluation tool in clinical medicine. Clin Chem 39:561–577
27. Tsuchiya R, Noda T, Harada N et al (1986) Collective review of small carcinomas of the pancreas. Ann Surg 203:77–81
28. Prokesch RW, Chow LC, Beaulieu CF, Bammer R, Jeffrey RB Jr (2002) Isoattenuating pancreatic adenocarcinoma at multi-detector row CT: secondary signs. Radiology 224:764–768
29. d'Assignies G, Couvelard A, Bahrami S et al (2009) Pancreatic endocrine tumors: tumor blood flow assessed with perfusion CT reflects angiogenesis and correlates with prognostic factors. Radiology 250:407–416
30. Bettini R, Partelli S, Boninsegna L et al (2011) Tumor size correlates with malignancy in nonfunctioning pancreatic endocrine tumor. Surgery 150:75–82
31. Caramella C, Dromain C, De Baere T et al (2010) Endocrine pancreatic tumours: which are the most useful MRI sequences? Eur Radiol 20:2618–2627